High-Cooperativity Coupling of Electron-Spin Ensembles to Superconducting Cavities

D. I. Schuster,[1] A. P. Sears,[1] E. Ginossar,[1] L. DiCarlo,[1] L. Frunzio,[1] J. J. L. Morton,[2] H. Wu,[2] G. A. D. Briggs,[2] B. B. Buckley,[3] D. D. Awschalom,[3] and R. J. Schoelkopf[1]

[1]*Department of Applied Physics and Physics, Yale University, New Haven, Connecticut 06511, USA*
[2]*Department of Materials, University of Oxford, Oxford OX1 3PH, United Kingdom*
[3]*Center for Spintronics and Quantum Computation, University of California, Santa Barbara, California 93106, USA*

(Received 18 June 2010; revised manuscript received 11 August 2010; published 27 September 2010)

Electron spins in solids are promising candidates for quantum memories for superconducting qubits because they can have long coherence times, large collective couplings, and many qubits could be encoded into spin waves of a single ensemble. We demonstrate the coupling of electron-spin ensembles to a superconducting transmission-line cavity at strengths greatly exceeding the cavity decay rates and comparable to the spin linewidths. We also perform broadband spectroscopy of ruby ($Al_2O_3 : Cr^{3+}$) at millikelvin temperatures and low powers, using an on-chip feedline. In addition, we observe hyperfine structure in diamond $P1$ centers.

DOI: 10.1103/PhysRevLett.105.140501 PACS numbers: 03.67.Lx, 42.50.Pq, 76.30.−v

An eventual quantum computer, like its classical analog, will make use of a variety of physical systems specialized for different tasks. Just as a classical computer uses charge-based transistors for fast processing and magnetic hard drives for long-term information storage, a quantum computer might use superconducting qubits for processing [1] and ensembles of electron spins as quantum memories [2,3], linked by single microwave photons. Although other microscopic systems have been proposed for use in a hybrid architecture [4–7], electron spins complement superconducting qubits particularly well. They feature similar transition frequencies, do not require trapping, and can be packed densely. Furthermore, a single ensemble could be used to store many qubits using holographic encoding [3], a technique used for classical microwaves using nuclear [8] and electron [9] spin ensembles.

In this Letter, we demonstrate the first step toward realizing a solid-state quantum memory: coupling an electron-spin ensemble to an on-chip superconducting cavity at powers corresponding to a single cavity photon. We observe megahertz spin-photon interaction strengths in both Cr^{3+} spins in Al_2O_3 (ruby) and N substitution ($P1$) centers in diamond. A parallel effort by Kubo *et al.* [10] sees similar coupling to nitrogen-vacancy (N-V) centers in diamond. The devices developed here can also serve as a platform for the investigation of electron-spin resonance (ESR) physics in picoliter mode volumes, millikelvin temperatures, and attowatt powers.

ESR studies the microwave response of electron spins in a magnetic field. Samples are conventionally placed inside a 3D high-quality-factor (Q) cavity which enhances the sensitivity by confining photons with the spins and extending the interaction time [11]. In this work, several 1D cavities are capacitively coupled to a common feedline on an Al_2O_3 (sapphire) chip. In the first experiment the cavities and feedline are fabricated on $Al_2O_3 : Cr^{3+}$ (ruby), on top of a half-space with a constant density of spins ρ. In the second experiment, a spin-containing sample of diamond is placed upon an existing device fabricated on undoped Al_2O_3 [Fig. 1(a)]. A cavity or feedline defines a zero-point magnetic field B_{ZP} which couples microwave

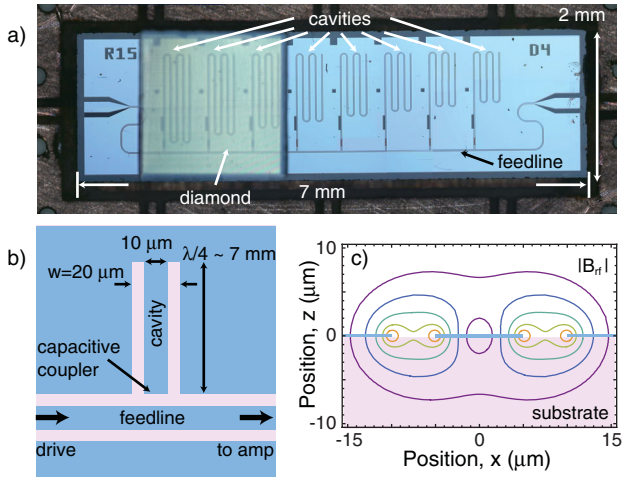

FIG. 1 (color). (a) Eight $\lambda/4$ cavities with fundamental frequencies from 4 to 8 GHz coupled to a common feedline fabricated on an Al_2O_3 substrate. A $2 \times 2 \times 1$ mm^3 chip of diamond is placed on top, synthetically grown with 1 ppm of nitrogen which form spin-active $P1$ centers. In a similar device spins are instead provided by Cr^{3+} doped directly into the Al_2O_3 substrate. (b) A simplified schematic top view of a single cavity. The actual cavities in (a) are meandered to make them more compact. The cavity frequency is determined by the length of the stub ~7 mm while the coupling Q is set by the capacitance of the coupler section. (c) Cross section of the coplanar waveguide showing contours of equal microwave magnetic field strength (B_{rf}). Each contour represents a factor of 2 in $|B_{rf}|$, such that only spins within a few microns above and below the surface see an appreciable field from the transmission line.

radiation to individual spins inside the mode volume with strength $g_s/\hbar = m_0 B_{\mathrm{ZP}}/\hbar$, where m_0 is the transition magnetic dipole moment. For small excitations, an ensemble of spins uniformly coupled to a microwave field behaves as a spin-harmonic oscillator, maintaining the original spin resonance frequency $\omega_s/2\pi$, but with an effective collective coupling strength $g_{\mathrm{eff}} = g_s\sqrt{N}$ [12]. A single spin at the center of one of the gaps in Fig. 1 will have a $g_s/2\pi \sim 65$ Hz, much too slow to couple to a superconducting qubit with microsecond decay times [13]. If $\sim 10^{12}$ spins were uniformly coupled, this could be enhanced to $g_{\mathrm{eff}}/2\pi \sim 65$ MHz, fast enough for many operations. In general the driving field or density will not be completely uniform throughout the sample. The basic spin-harmonic oscillator approximation is still valid with the expression for the coupling generalized to $g_{\mathrm{eff}} = \frac{m_0}{\hbar}\sqrt{\mu_0\hbar\omega_c\rho\nu/4}$, where the cavity frequency is $\omega_c/2\pi$ and the filling factor is

$$\nu = \int |\vec{B}_{\mathrm{ZP}}(\vec{r}) \times \hat{S}|^2 dV_{\mathrm{sample}} \Big/ \left(\int |\vec{B}_{\mathrm{ZP}}(\vec{r})|^2 dV \right). \quad (1)$$

For these samples $\nu \sim 0.25$ due to half the plane being filled with spins and another factor of one-half from the angle between the static and microwave magnetic fields. While the single spin coupling depends on the cavity mode volume, the ensemble coupling depends only on ρ, ω_c, and the dimensionless ν. Thus, for these experiments the small mode volume of the cavities is not paramount; however, to maintain reasonable values of ν for small samples it can be helpful to shrink the cavity mode volume as has been done in several "micro-ESR" experiments [14–16]. A superconducting cavity, as described here, is able to maintain high Q at the extreme aspect ratios (350) associated with small mode volumes, even at applied in-plane fields >200 mT [17].

The $Al_2O_3 : Cr^{3+}$ device [Fig. 1(a)] consists of several $\lambda/4$ cavities capacitively coupled to a common broadband feedline. Both components are made from sections of coplanar waveguide transmission line, which act as 2D versions of coaxial cables [see Figs. 1(a) and 1(b)]. The microwave fields from the transmission lines extend only a few microns into the substrate [see Fig. 1(c)]. There are thus several spatially separated, independent ensembles of spins. First, there is an ensemble within a tube of 20 μm radius below the feedline that runs the length of the chip (~1 cm). Second, there is an ensemble beneath each meandering cavity (~7 mm). Finally, there are spins in the bulk which do not couple directly to the on-chip elements but interact with sample box resonances.

All of these interactions must be considered in Fig. 2 where transmission through the feedline is measured over a wide frequency range (10–14.5 GHz) as a function of the in-plane magnetic field. Absorption lines from spins interacting with the feedline are visible over the whole band and are due to transitions of the Cr^{3+} dopants. They are accurately modeled by diagonalizing the single spin

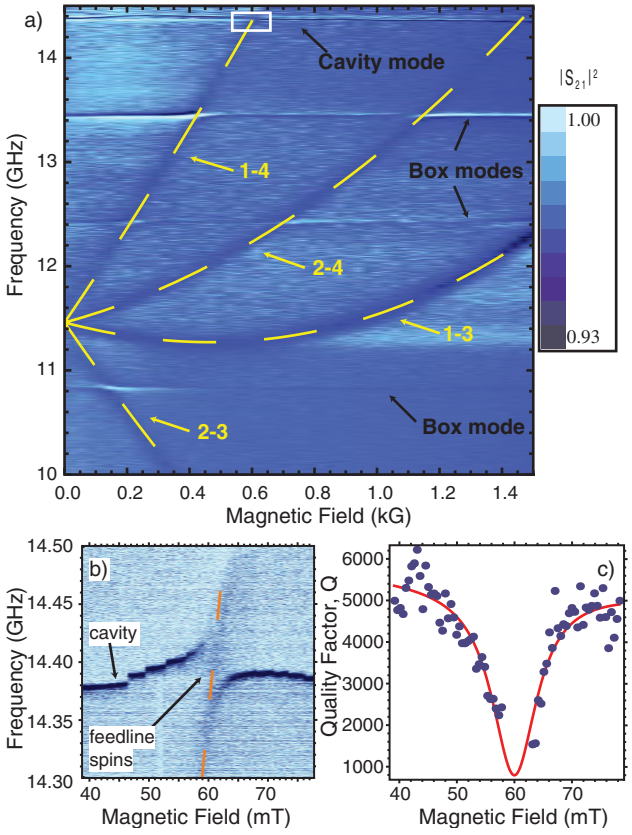

FIG. 2 (color). Transmission spectroscopy of ruby ($Al_2O_3 : Cr^{3+}$) sample in a parallel magnetic field. (a) The dashed curves are transitions between labeled energy levels of the Cr^{3+} spins. The fit uses only two parameters, the magnet current to field ratio and the angle between the magnetic field and crystal $\hat{c}$ axis which is found to be 64.6°. To compensate for frequency dependent attenuation in the microwave lines, each point is divided by the mean of all points with the same frequency (row). The three broad horizontal lines are resonances with the copper sample box. The narrow line at ~14.35 GHz is the second mode of the longest superconducting cavity. (b) Higher resolution scan where the $1 \leftrightarrow 4$ transition intersects the cavity resonance. The nearly vertical feature at 60 mT is due to the spins coupled to the feedline. An avoided crossing with the superconducting cavity is visible, indicating coupling to $N \approx 4 \times 10^{12}$ spins. The abrupt jumps in the cavity frequency are thought to be due to flux penetrating the superconducting film causing changes in the effective inductance of the cavity. (c) Fit using Eq. (2), to the Q of the cavity, which is partially damped by the spins.

Hamiltonian [18], $H_r = -m_{0,r}\vec{B} \cdot \vec{S} - D(S_z^2 - 5/4)$, with $m_{0,r}/2\pi = 27.811$ MHz/mT, $\vec{S}$ the spin-3/2 operator, $\hat{z}$ is defined along the $\hat{c}$ crystal axis, and $2D/2\pi = 11.46$ GHz. In addition to the Zeeman term, there is a large crystal field in $Al_2O_3 : Cr^{3+}$ that separates the levels into two doublets ($S_z = \pm 3/2$ and $S_z = \pm 1/2$). The measured spectroscopic lines correspond to transitions between the doublets and are labeled by the energy levels involved in the tran-

sition. When a magnetic field is applied at an angle with respect to the $\hat{c}$ axis the levels within each doublet are hybridized and give the observed curvature in the transitions. Because of the relatively high doping $\sim 10^{19}$–10^{20} cm^{-3} and ~ 1 cm length of the feedline, absorption at the transition frequencies of the Cr^{3+} spins is visible even without the aid of a cavity. From the 5% absorption dips we estimate that there are approximately 10^{13} spins interacting with the feedline.

In addition to the spectrum of spins coupled to the feedline, several magnetic field-insensitive resonances (horizontal lines) are evident in Fig. 2(a). The bottom three broad modes are resonances in the sample box, while the narrow mode at 14.35 GHz is the first superconducting transmission-line cavity. The modes of both the copper sample box and the superconducting cavities interact with their respective spin ensembles, but we focus on the on-chip cavities which are higher Q and have been shown to couple strongly to superconducting qubits [19].

In a higher-resolution scan [Fig. 2(b)] an avoided crossing is present where the transition between the ground state and highest energy level of the Cr^{3+} spin (1–4) approaches the cavity at 14.35 GHz. Also visible are spins interacting with the feedline but not the cavity mode and thus have no level repulsion. Both effects are visible, indicating they are due to independent spin ensembles. The cavity line in Fig. 2(b) is repelled by more than its linewidth, and on resonance is damped primarily by the spins. Because of jumps in the cavity frequency near the crossing attributed to penetration of magnetic flux vortices into the superconducting film, it is difficult to precisely fit frequency versus field. However, the Q of the cavity is relatively unaffected by these jumps, and is used to extract the same information in Fig. 2(c).

The Q of a cavity coupled to an ensemble of spins is

$$Q = \frac{\Delta^2 + \gamma_2^{*2}}{2g_{s,\mathrm{eff}}^2 \gamma_2^* + \kappa(\Delta^2 + \gamma_2^{*2})}\omega_r, \qquad (2)$$

where both the ensemble of spins and the cavity are modeled as single-mode harmonic oscillators with detuning Δ, cavity frequency $\omega_r/2\pi = 14.35$ GHz, and spin frequency degenerate at $B = 60$ mT. The spin resonance tunes at rate $m_{\mathrm{eff}}/2\pi = 52.4$ MHz/mT. Equation (2) is valid so long as one of Δ, γ_2^*, or κ is much larger than $g_{s,\mathrm{eff}}$, and for this reason the few points right at degeneracy are not used in Fig. 2(b). The cavity linewidth $\kappa/2\pi = \omega_r/2\pi Q = 1.3$ MHz is independently measured away from resonance. The collective coupling strength, $g_{s,\mathrm{eff}}/2\pi = 38$ MHz, and spin linewidth, $\gamma_2^*/2\pi = 96$ MHz, are extracted from the fit. The latter is probably primarily due to broadening by strong hyperfine interactions with ^{27}Al nuclear spins [20] with some contributions due to dipolar broadening and field inhomogeneity. The coupling is much larger than the decoherence rates measured in both the cavity and typical superconducting qubits [1]. A dimensionless measure of the coupling strength in cavity QED [21] is the cooperativity $C = g^2/\kappa\gamma_2^* \approx 11.5$. Since $C > 1$, the coupling is strong in the sense that at resonance nearly every photon entering the cavity is coherently transferred into the spins. Retrieving the photon will require a spin system with smaller linewidth.

Using the diamond sample we are able to observe hyperfine splittings which could eventually be used to transfer information from electron to nuclear spins. ESR active $P1$ centers [22] are visible via absorption spectroscopy (Fig. 3), but we did not observe N-V centers.

The observed splittings can be understood by considering the transitions of the Hamiltonian [22] $H_d = -m_{0,d}\vec{B}\cdot\vec{S} + A\vec{S}\cdot\vec{I}$, where $m_{0,d}/2\pi = 28.04$ MHz/mT and the hyperfine coupling tensor $A/2\pi = (81.33, 81.33, 114.03)$ MHz. Here, the $\hat{z}$ direction corresponds to the diamond $\langle 111\rangle$ axis, $\vec{S}$ are the electron spin-1/2 operators, and $\vec{I}$ are the nuclear spin-1 operators. This describes a nitrogen atom with an extra, nearly free electron, and a hyperfine spectrum due to the $I = 1$ nuclear spin of ^{14}N. This splits the line into three: $m_I = -1, 0, 1$. Anisotropy in the hyperfine coupling can split the spectrum further, but when the bias field is applied along $\langle 100\rangle$ all of the carbon bonds make equivalent angles with the $\vec{B}$ field, and so only three lines are visible.

For $N \gg 1$ and low excitation powers, the collective spins $J^{(n)}$ couple to the cavity as a set of independent harmonic oscillators with frequencies ω_n, and decay rate γ_2^*, where n indexes the transitions. Each of the three hyperfine transitions is treated as an independent spin-

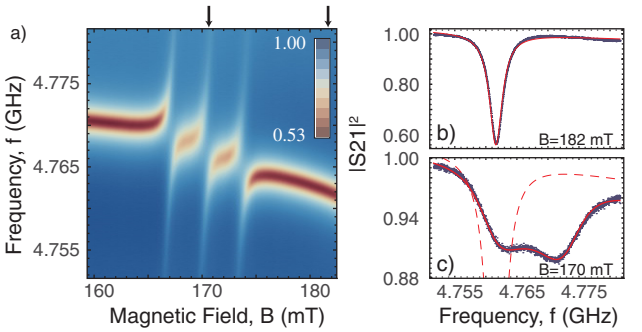

FIG. 3 (color). Transmission spectrum of $P1$ centers in diamond. The density plot (a) shows three avoided crossings corresponding to the electron-spin transitions which conserve the ^{14}N nuclear spin $m_I = -1, 0, 1$. Line cuts are taken away from the crossing (b) showing the bare cavity and at the central feature (c) showing the interactions with the spins. From the fit to Eq. (3) (solid red line) the cavity is found to have external coupling $\kappa_c/2\pi = 300$ kHz, internal loss rate $\kappa_i/2\pi = 1.8$ MHz, and total linewidth $\kappa/2\pi = (\kappa_i + \kappa_c)/2\pi = 2.1$ MHz. At the center of the crossing (c), the cavity and spin systems hybridize giving a double-peaked spectrum, with a splitting $2g/2\pi = 16.2$ MHz and spin linewidth $\gamma_2^*/2\pi = 19.7$ MHz.

harmonic oscillator with each ensemble uniformly coupled to the cavity at rate g. Because the diamond sample has less overlap with the feedline, its absorption signal is not evident in Fig. 3. The full transmission spectrum can be calculated using input-output formalism [23] to be

$$|S_{21}|^2 = \left| 1 + \frac{\kappa_c}{i(\omega - \omega_r) - (\kappa_c + \kappa_i) + \sum_n \frac{|g|^2}{i(\omega - \omega_n) - \gamma_2^*/2}} \right|^2, \quad (3)$$

where κ_c and κ_i are the external and internal dissipation rate of the cavity, respectively. The g and linewidths are extracted from fits to Eq. (3) in Figs. 3(b) and 3(c) with the simplification that only one of the spin ensembles contributes significantly near each resonance. The cooperativity is $C = g^2/\kappa\gamma_2^* \sim 1.6$. The coupling strength is similar to the spin linewidth and greatly exceeds dissipation rates for superconducting qubits and cavities [13]. The spin linewidth is most likely due to dipolar broadening [24] or magnetic field inhomogeneity.

To realize a quantum spin memory several improvements must be made. Most importantly, a more coherent electron-spin candidate is required. In addition, because superconducting qubits might be adversely affected by magnetic fields, an ideal candidate would have a large zero-field splitting such that at $B = 0$, $\hbar\omega \gg k_B T$, which could come from crystal field splittings as with the $Al_2O_3 : Cr^{3+}$ shown here and N-V^- centers, or other effects like hyperfine coupling. In addition, line broadening due to dipolar couplings, nuclear spins, strain variations, and inhomogeneous bias fields must be controlled. New cavity designs could improve the static and microwave magnetic field uniformities, allowing spin-echo techniques to be applied. It may even be possible to achieve strong coupling with single spins if superconducting qubits can be used to mediate the interactions [25,26].

The system also shows promise as a general ESR tool with good sensitivity in a broadband system, and exquisite sensitivity in a high-Q cavity. The small mode volume makes it ideally suited for studying picoliter scale samples, especially 2D systems such as graphene or semiconducting heterostructures. Further, because the device can maintain good sensitivity even when the cavity is excited with a single photon at a time (typically $\sim$1 aW), it can be used to study ESR at millikelvin temperatures where cooling power is limited. Measuring at such low powers facilitates studies of samples with inconveniently long T_1 (common at millikelvin temperatures), because they can be probed for hours before saturating the spins.

We have demonstrated coupling of large ensembles of electron spins to both broadband coplanar waveguide feedlines and cavities. The coupling is sufficiently strong to exceed all qubit and cavity decay rates with large cooperativity, but the system's use as a quantum memory is still limited by the spin linewidth. Further applications could include maser amplification and single-photon microwave to optical up-conversion.

The authors would like to acknowledge P. Doering at Apollo Diamond for providing a synthetic diamond sample used in preliminary studies, G. Ulas for help performing room temperature ESR, as well as discussions with S. Lyon, M. Reed, and G. Brudvig. We acknowledge support for this work from NSF DMR-0653377, AFOSR (B. B. D., D. D. A.), Yale University (D. I. S.), CNR-Istituto di Cibernetica (L. F.), and the UK Royal Society (J. J. L. M.).

[1] L. DiCarlo *et al.*, Nature (London) **460**, 240 (2009).
[2] A. Imamoglu Phys. Rev. Lett. **102**, 083602 (2009).
[3] J. H. Wesenberg *et al.*, Phys. Rev. Lett. **103**, 070502 (2009).
[4] M. Wallquist *et al.*, Phys. Scr. **T137**, 014001 (2009).
[5] J. M. Taylor, C. M. Marcus, and M. D. Lukin, Phys. Rev. Lett. **90**, 206803 (2003).
[6] J. Verdu *et al.*, Phys. Rev. Lett. **103**, 043603 (2009).
[7] A. Andre *et al.*, Nature Phys. **2**, 636 (2006).
[8] A. G. Anderson *et al.*, J. Appl. Phys. **26**, 1324 (1955).
[9] H. Wu *et al.*, Phys. Rev. Lett. **105**, 140503 (2010).
[10] Y. Kubo *et al.*, Phys. Rev. Lett. **105**, 140502 (2010).
[11] J. A. Weil and J. R. Bolton, *Electron Paramagnetic Resonance* (Wiley, New York, 2007), p. 548.
[12] R. H. Dicke, Phys. Rev. **93**, 99 (1954).
[13] J. A. Schreier *et al.*, Phys. Rev. B **77**, 180502 (2008).
[14] W. J. Wallace and R. H. Silsbee, Rev. Sci. Instrum. **62**, 1754 (1991).
[15] G. Boero *et al.*, Rev. Sci. Instrum. **74**, 4794 (2003).
[16] R. Narkowicz *et al.*, Rev. Sci. Instrum. **79**, 084702 (2008).
[17] H. J. Mamin *et al.*, Rev. Sci. Instrum. **74**, 2749 (2003).
[18] J. Weber, Rev. Mod. Phys. **31**, 681 (1959).
[19] A. Wallra *et al.*, Nature (London) **431**, 162 (2004).
[20] N. Laurance *et al.*, J. Phys. Chem. Solids **23**, 515 (1962).
[21] D. Walls and G. J. Milburn, *Quantum Optics* (Springer, New York, 2008), Chap. 11, pp. 213–227.
[22] J. H. N. Loubser and J. A. van Wyk, Rep. Prog. Phys. **41**, 1201 (1978).
[23] A. A. Clerk *et al.*, Rev. Mod. Phys. **82**, 1155 (2010).
[24] J. V. Wyk, E. Reynhardt, G. High, and I. Kiawi, J. Phys. D **30**, 1790 (1997).
[25] J. Twamley and S. D. Barrett, Phys. Rev. B **81**, 241202 (2010).
[26] D. Marcos *et al.*, arXiv:1001.4048.